JCTC Journal of Chemical Theory and Computation
Letter
pubs.acs.org/JCTC

Accuracy of Current All-Atom Force-Fields in Modeling Protein Disordered States

Ferruccio Palazzesi,*[,†,‡] Meher K. Prakash,[¶] Massimiliano Bonomi,[§] and Alessandro Barducci*[,∥]

[†]Department of Chemistry and Applied Biosciences, Eidgenössische Technische Hochschule Zürich, CH-8093 Zurich, Switzerland
[‡]Facoltá di Informatica, Istituto di Scienze Computazionali, Universitá della Svizzera Italiana, 6900 Lugano, Switzerland
[¶]Theoretical Sciences Unit, Jawaharlal Nehru Centre for Advanced Scientific Research, Jakkur, Bangalore, Karnataka, 500064, India
[§]Department of Chemistry, University of Cambridge, Lensfield Road, Cambridge CB2 1EW, United Kingdom
[∥]Laboratoire de Biophysique Statistique, École Polytechnique Fèdèrale de Lausanne (EPFL), CH-1015 Lausanne, Switzerland

Supporting Information

ABSTRACT: Molecular Dynamics (MD) plays a fundamental role in characterizing protein disordered states that are emerging as crucial actors in many biological processes. Here we assess the accuracy of three current force-fields in modeling disordered peptides by combining enhanced-sampling MD simulations with NMR data. These force-fields generate significantly different conformational ensembles, and AMBER03w [Best and Mittal *J. Phys. Chem. B* **2010**, *114*, 14916−14923] provides the best agreement with experiments, which is further improved by adding the ILDN corrections [Lindorff-Larsen et al. *Proteins* **2010**, *78*, 1950−1958].

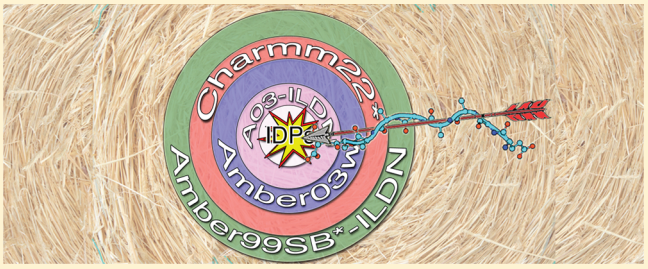

1. INTRODUCTION

Molecular dynamics (MD) simulations are currently a valuable tool for studying complex biomolecular systems as they provide an atomistic description of their structure and dynamics. Unfortunately, MD predictive capabilities are limited by two factors: the accuracy of the molecular mechanics force-fields and the complexity of biomolecular free-energy landscapes, which often make exhaustive sampling by means of standard MD a daunting task. The use of specialized hardware[1] and distributed computing platforms[2] as well as the development of advanced sampling algorithms[3] have significantly alleviated this time scale limitation. As a consequence of these developments, the community is increasingly focusing on the creation of more accurate force-fields, as demonstrated by the large number of works aimed at comparing the quality of different force-fields,[4−12] and the number of corrections recently proposed.[13−17]

MD simulations currently play a key role in investigating disordered states of proteins, whose biological importance is increasingly recognized. Indeed, intrinsically disordered proteins (IDPs), which do not adopt a well-defined three-dimensional structure under physiological conditions, represent a significant fraction of any proteome and they are important actors in essential biological processes such as signaling and regulation.[18,19] Furthermore, the conformational flexibility of specific protein fragments is often crucial in mediating allosteric signal propagation[20−22] and protein−protein interactions in structured proteins.[23,24] The highly dynamic and conformationally heterogeneous nature of protein disordered states creates significant difficulties to most of the experimental structural biology techniques. NMR spectroscopy is probably the most comprehensive approach for studying these states and several NMR observables, such as chemical shifts, scalar couplings (^{3}J-couplings), and residual dipolar couplings (RDCs), provide precious information about the average conformational properties of disordered proteins, both at the local and global level. However, the translation of this experimental data into ensembles of detailed structures invariantly relies on computational protocols[25,26] that are often based on MD simulations.[27,28] The reliability of force-fields in reproducing the correct conformational distributions of disordered proteins is thus an essential ingredient to improve our understanding of many relevant biological processes.

Here we tested the accuracy of current force-fields in modeling a set of disordered peptides that were previously characterized by NMR spectroscopy.[29] In order to guarantee an exhaustive exploration of their conformational landscapes, we adopted an advanced simulation protocol based on metadynamics (MetaD).[30,31] The resulting structural ensembles were validated by calculating several NMR observables ($^3J_{HNHA}$-couplings, CA and N chemical shifts, and N−H RDCs) and comparing them with experimental data.

Received: August 7, 2014
Published: December 12, 2014

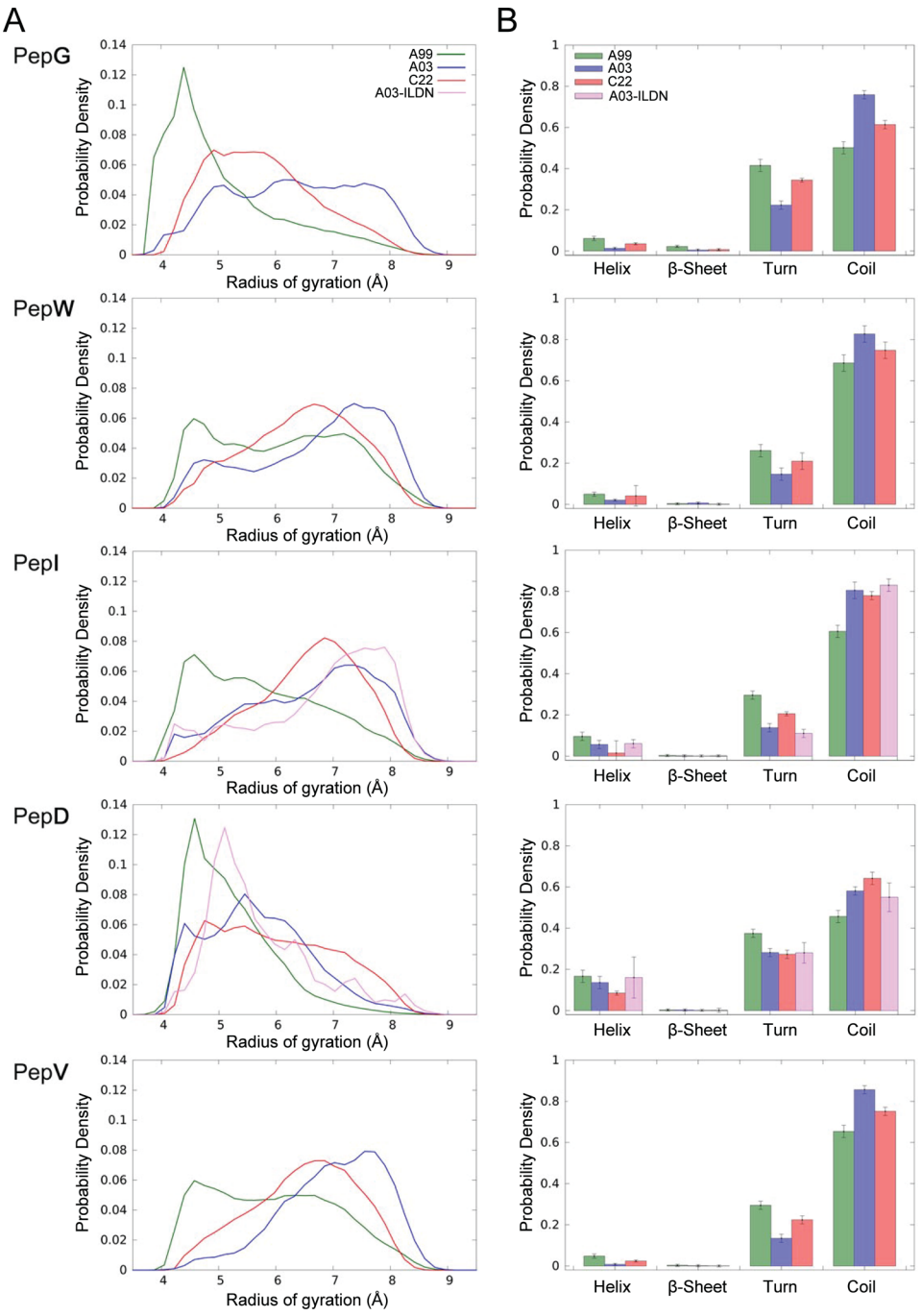

Figure 1. Rg (Panel A) and secondary structure (Panel B) distributions calculated on the conformational ensemble generated by A99 (green), A03 (blue), C22 (red), and A03-ILDN (pink), for each of the 5 peptides. The vertical black lines indicate the errors calculated with the approach in ref 62.

2. RESULTS AND DISCUSSION

As model systems of protein disordered states, we chose unstructured peptides of sequence EGAAXAASS, which have been extensively investigated by Grzesiek and co-workers[29] by means of NMR spectroscopy. Here we focused on 5 sequences, with X corresponding to G, W, I, D, and V (PepG, PepW, PepI, PepD, and PepV, respectively). This set, although limited, allowed us to sample the conformational preferences induced by amino acids of diverse hydrophobicity and size. We considered three state-of-the-art force-fields optimized for biomolecular simulations: AMBER99SB*-ILDN[13,14] (A99), CHARMM22*[11] (C22), and AMBER03w[32] (A03). These force-fields were used in combination with an explicit solvent description based on appropriate water models: TIP3P,[33] TIPS3P (or mTIP3P),[34] and TIP4P/2005[35] for A99, C22, and A03, respectively. Notably, A99 and C22 were recently ranked as the most accurate force-fields on the basis of MD simulations beyond the microsecond time scale,[9] and A03 was shown to provide an improved description of unfolded states in combination with the TIP4P/2005 water model.[32] Additionally, we tested the effect of the ILDN side-chain dihedral corrections,[13] originally developed for AMBER99SB,[36] on modeling PepI and PepD with A03. Average properties of the conformational ensemble generated by this hybrid force-field

dx.doi.org/10.1021/ct500718s | J. Chem. Theory Comput. 2015, 11, 2−7

(A03-ILDN) were obtained *a posteriori* by reweighting the simulations carried out with A03, see the Supporting Information (SI).

Efficient sampling of the configurational landscapes was achieved by using PT-WTE, which combines the Parallel Tempering (PT)[37] and Well-Tempered Ensemble (WTE)[38] approaches. With PT-WTE, sampling is enhanced by enlarging the fluctuations of the potential energy with a time-dependent bias potential,[39] thus reducing the number of replicas needed by PT to span a given temperature range in explicit-solvent simulations. Previous applications demonstrated the efficiency of this protocol to accelerate sampling of standard MD.[22,40,41]

In order to characterize the conformational ensembles generated by each combination of peptide and force-field, we reported the distributions of the radius of gyration (Rg) and secondary structure content[42] (Figure 1). This analysis suggested that some structural features were observed for all the peptides independently of the force-field. Indeed, the broad distributions of Rg (Figure 1A) indicated that the peptides were significantly flexible, and they could adopt both extended and compact conformations. Moreover, these conformations were mostly disordered, as suggested by a strong preference of coil and turn structures, a small helical population, and a negligible β-sheet content (Figure 1B). However, the shapes of the distributions in Figure 1A revealed that the conformational ensembles generated by the various force-fields presented notable differences. In particular, A99 favored more compact conformations with respect to A03 and C22 for all peptides, as confirmed by the average values of Rg (Table 1). These compact ensembles were characterized by a higher average number of backbone−backbone hydrogen bonds (H-bonds) (Table 1) leading to a larger content of turns and helices (Figure 1B). This result is in agreement with the force-field dependence of the unfolded state of other proteins.[9]

Table 1. Average of the Structural Measures (Rg, H-Bonds, and Secondary Structure Content) on the Conformational Ensembles Generated by the Different Force-Fields for Each of the 5 Peptides Studied

				secondary structure			
peptides	force-fields	Rg (Å)	H-bonds	helix	β-sheet	turn	coil
PepG	A99	5.2	2.1	0.06	0.02	0.41	0.50
	A03	6.4	1.3	0.01	<0.01	0.22	0.76
	C22	5.9	1.4	0.03	0.01	0.34	0.61
PepW	A99	6.2	1.8	0.05	<0.01	0.26	0.69
	A03	6.8	1.6	0.02	<0.01	0.15	0.83
	C22	6.5	1.4	0.04	<0.01	0.21	0.75
PepI	A99	5.9	1.9	0.09	<0.01	0.30	0.60
	A03	6.7	1.5	0.05	<0.01	0.14	0.80
	C22	6.7	1.2	0.01	<0.01	0.20	0.78
	A03-ILDN	6.9	1.4	0.06	<0.01	0.11	0.83
PepD	A99	5.3	2.5	0.17	<0.01	0.37	0.46
	A03	5.8	2.0	0.13	<0.01	0.28	0.58
	C22	6.1	1.5	0.08	<0.01	0.27	0.64
	A03-ILDN	5.8	2.1	0.16	<0.01	0.28	0.55
PepV	A99	6.0	1.7	0.05	<0.01	0.29	0.65
	A03	7.1	1.2	0.01	<0.01	0.13	0.86
	C22	6.6	1.2	0.02	<0.01	0.22	0.75

The differences between A03 and C22 were more subtle. A03 generated in three cases out of five the most extended ensembles (Figure 1A), which were characterized by a higher percentage of coil structure (Figure 1B) and consequently a smaller number of H-bonds (Table 1). In the case of PepI, our structural measures were similar for A03 and C22, while C22 generated a more extended ensemble in the case of PepD. This scenario was not altered by introducing the ILDN corrections to A03. Indeed, a slight increase of Rg and a decrease of the average number of H-bonds were observed for PepI, while PepD was substantially unaffected (Table 1). A similar trend among force-fields was observed using other structural measures (Figures S1 and S2).

Our structural analysis highlighted substantial differences in the conformational ensembles generated by each force-field. However, to determine which force-field generates the more accurate conformational ensemble, we calculated several NMR observables from our simulations and compared them with available experimental data.[29] In particular, we focused here on the $^3J_{HNHA}$-couplings, the CA and N chemical shifts, and the N−H RDCs.

The $^3J_{HNHA}$-couplings are related to the ϕ backbone dihedral angle, and thus they are assumed to correlate with the secondary structure population. We used the Karplus equation[43] with the "ubiquitin" set of parameters[44,45] (Ubq) to compute the $^3J_{HNHA}$-couplings from our simulations, and their Root-Mean Square Deviation (RMSD) from the measured couplings was used to quantify the agreement with experiments. In Figure 2A we reported the RMSDs calculated for each peptide and force-field combination along with the average deviations associated with each force-field. Raw data is in Table 2. It is reassuring that the RMSDs calculated with these last generation force-fields are smaller than the typical error of previous, less-optimized force-fields,[12,46] although they are still greater than the reported accuracy of the Ubq set of parameters. The poorest average agreement with experimental couplings was found in the case of C22, while A03 provided the best estimates of this observable. This agreement was further improved, in particular for PepD, by introducing the ILDN corrections to A03 (Figure S4). The observed trend was robust with respect to the choice of parameters in the Karplus equation (Figure S3).

Chemical shifts are another popular tool to characterize disordered proteins. Furthermore, chemical shifts measured on different nuclei are sensitive to different structural properties and thus may provide independent information about the conformational ensemble. In order to make contact with experiments, we calculated the CA and N chemical shifts from our simulations using Shiftx2,[47] which was shown to outperform other predictors on a benchmark set of 61 proteins (http://www.shiftx2.ca/performance.html). Similarly to what is done for the $^3J_{HNHA}$-couplings, we reported in Figure 2B the RMSDs from experimental data for each peptide and force-field combination along with the average deviations associated with each force-field. Raw data is in Table 2. We observed an excellent agreement between calculated and experimental CA chemical shifts, which was very weakly dependent on the force-field. However, this observable did not provide reliable information about the relative accuracy of the force-fields, since the average RMSDs were lower than the method accuracy in almost all cases. On the contrary, the deviations between calculated and experimental N chemical shifts were greater than the predictor accuracy, thus making the differences among force-fields significative. In particular, the more expanded ensembles generated by C22, A03, and A03-ILDN resulted in a

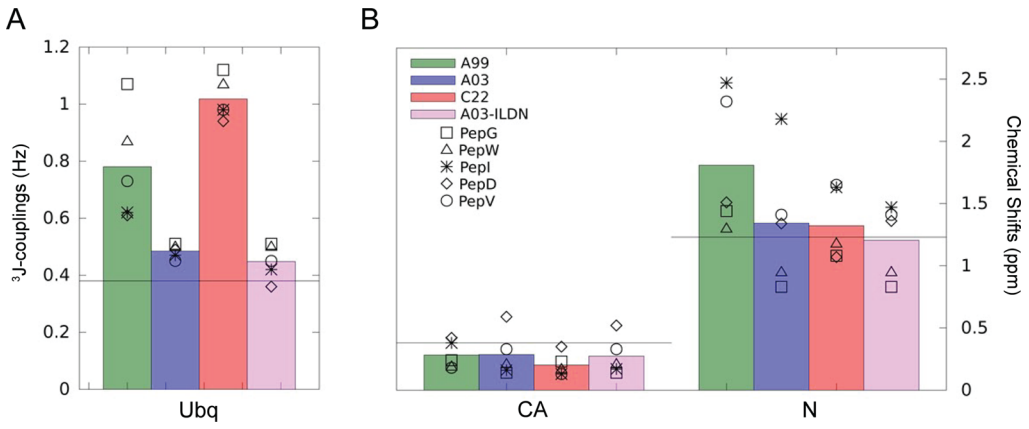

Figure 2. RMSD between simulated and experimental data for the $^3J_{HNHA}$-couplings (Panel A) and CA and N chemical shifts (Panel B). Bars indicate the average RMSD on the 5 peptides studied for each of the force-fields tested: A99 (green), A03 (blue), C22 (red), and A03-ILDN (pink). Symbols indicate the RMSD of a given peptide: PepG (square), PepW (triangle), PepI (star), PepD (diamond), and PepV (circle). The horizontal black lines indicate the typical predictor errors.

Table 2. Agreement between Experimental and Calculated NMR Observables for Each Peptide and Force-Field Studied[a]

			chemical shifts (ppm)		
peptides	force-fields	$^3J_{HNHA}$-couplings (Hz)	CA	N	RDCs
PepG	A99	1.07	0.24	1.36	0.45
	A03	0.51	0.14	0.83	0.37
	C22	1.12	0.23	1.08	0.89
PepW	A99	0.87	0.19	1.30	0.22
	A03	0.50	0.21	0.95	0.45
	C22	1.07	0.17	1.18	0.67
PepI	A99	0.62	0.38	2.47	0.13
	A03	0.47	0.16	2.18	0.10
	C22	0.98	0.13	1.63	0.20
	A03-ILDN	0.42	0.17	1.47	0.16
PepD	A99	0.61	0.42	1.52	0.11
	A03	0.49	0.59	1.34	0.27
	C22	0.94	0.35	1.07	0.06
	A03-ILDN	0.36	0.52	1.36	0.04
PepV	A99	0.73	0.18	2.32	0.01
	A03	0.45	0.33	1.41	0.30
	C22	0.98	0.13	1.65	0.11
	method error (RMSD)	**0.39**	**0.38**	**1.23**	

[a]Deviations are quantified by RMSD for $^3J_{HNHA}$-couplings and chemical shifts (the lower the better) and by the Pearson Coefficient for RDCs (the higher the better). The typical error of the predictor is reported at the bottom of the table.

better agreement with experimental data than the compact ensembles obtained with A99. Notably, the ILDN corrections to A03 lead to a consistent improvement in the agreement of the PepI N chemical shifts. This was not unexpected, because these chemical shifts can be influenced by the conformational dynamics of the side-chain χ angles,[48,49] which are greatly affected by the ILDN corrections. These corrections influenced not only the Ile or Asp chemical shifts but also the neighboring residue (Figure S5). A lack of an analogous improvement in PepD might be attributed to the smaller effect of the ILDN corrections on the rotameric distribution of Asp side chain.[13] A similar trend of relative accuracies among force-fields was observed with other predictors, although their smaller accuracies limited the statistical significance of the results (Figures S6 and S7).

Recently, RDCs have been widely exploited to characterize the conformational ensembles of IDPs.[50] At variance with the ^{3}J-couplings and chemical shifts, which are sensitive to the local physicochemical environment, RDCs provide long-range informations as they depend on the relative orientation of the system with respect to an alignment medium. RDCs were calculated from our simulations using PALES[51] and the steric module to determine the alignment tensor (SI). The agreement between simulations and experimental data was quantified by the Pearson's Correlation Coefficient (PCC) for each system and force-field studied (Table 2). On average, the agreement was extremely limited, except for the case of PepG modeled with C22 (PCC > 0.80). A poor correlation between calculated and experimental RDCs was not totally unexpected as similar results were obtained in previous studies of other unstructured systems.[52,53] These discrepancies might be due to the nature of this NMR observable, which it is expected to be dramatically sensitive to the alignment tensor determined by the overall conformation of the system. Thus, in the case of extremely flexible systems that sample several comparably populated states, small inaccuracies of the force-field and of the predictor are likely to result in large deviations of the calculated RDCs from experiments. For these reasons, we did not include this observable in our analysis of the force-fields.

3. CONCLUSION

Here we assessed the accuracy of current force-fields in simulating model systems characterized by the lack of a well-defined stable structure. This class of proteins plays a crucial role in many essential biological processes, and MD simulations can be instrumental in characterizing their structural properties, provided that sampling of the conformational landscape is exhaustive and force-fields are accurate. We overcame the sampling problem by using the PT-WTE algorithm, which combines the advantages of MetaD and PT. The three force-fields examined here generated conformational ensembles with significantly different structural properties. The comparison of these ensembles with NMR data, in particular ^{3}J-couplings and chemical shifts, revealed that A03 provides on average a more accurate description of these disordered systems. This

dx.doi.org/10.1021/ct500718s | J. Chem. Theory Comput. 2015, 11, 2−7

description can be further improved by incorporating the side-chains ILDN corrections originally developed for the AMBER99SB force-field. The quality of the agreement with experimental data could not be interpreted in terms of simple structural properties of the simulated ensembles, such as compactness and secondary structure content, and it most likely depended on a more subtle balance between inter- and intramolecular force-fields contributions.

4. COMPUTATIONAL METHODS

All simulations were carried out with Gromacs 4.5.6[54] and PLUMED 1.3.[55] Peptides were solvated in a dodecahedron periodic box with using about 1600 water molecules (Table T1). After equilibration (SI), all systems were simulated using the PT-WTE protocol with 8 replicas, which were properly distributed[56] in the range of 273−650 K. The WTE bias was constructed by depositing one Gaussian of width equal to 47.77 kcal/mol and initial height equal to 0.59 kcal/mol every picosecond. To ensure a sufficient overlap between energy distributions of neighboring replicas, we set the biasfactor equal to 40. Using this setup, we performed 200 ns of PT-WTE simulation per replica (20 ns further equilibration +180 ns production run) for a total of 1.6 μs for each system. Convergence was assessed by calculating the number of clusters found as a function of simulation time (Figure S8) and the Ramachandran plot distributions for each residue in the first and second half of all simulations (Figures S9−S13).

The equilibrium distributions of conformational variables can be obtained from the biased WTE simulation by means of an appropriate reweighting schemes.[57] However, the perturbation induced by the WTE bias on the solute conformational distribution was negligible (Tables T7 and T8), as previously noted for other solvated systems.[58] All the NMR observables (^{3}J-couplings, Chemical Shifts, and RDCs) were calculated from our simulations as ensemble averages. As routinely done in the case of disordered proteins, we assumed that (i) all the peptide conformers sampled by MD equally contribute to the ensemble average and (ii) these contributions are best estimated from the structure of individual conformers using the predictors described in the Results and Discussion section. It must be noted that most ^{3}J-couplings and Chemical Shifts predictors are empirically parametrized for folded proteins of known average structure and thus implicitly absorb a certain degree of motional averaging due to native-ensemble fluctuations.[59] However, we observed no significant differences when using J-couplings predictors that circumvent this issue by taking advantage of quantum calculation[60] or MD simulations[61] (Figure S3).

Statistical errors relative to structural measures and NMR observables were estimated using block-averaging[62] (Tables T9−T12).

■ ASSOCIATED CONTENT

Supporting Information

Further details of the MD protocol, the procedures for calculating structural properties and NMR observables from the MD trajectories, and convergence and error analysis. This material is available free of charge via the Internet at http://pubs.acs.org.

■ AUTHOR INFORMATION

Corresponding Authors

*Phone: +41216930513. Fax: +41216930523. E-mail: alessandro.barducci@epfl.ch.

*Phone: +41 (0)58 6664804. Fax: +41 (0)58 6664817. E-mail: ferruccio.palazzesi@phys.chem.ethz.ch.

Notes

The authors declare no competing financial interest.

■ ACKNOWLEDGMENTS

We thank Prof. Stephan Grzesiek (Biozentrum Basel) for providing chemical shifts data and for useful discussions, and Prof. Michele Parrinello (ETH Zürich - USI) for reading the manuscript and for providing a number of useful suggestions. A.B. thanks the Swiss National Science Foundation for financial support under the Ambizione grant PZ00P2_136856. Calculations were carried out on the Rosa supercomputer at the Swiss National Supercomputing Center (CSCS) under project ID s223.

■ REFERENCES

(1) Klepeis, J. L.; Lindorff-Larsen, K.; Dror, R. O.; Shaw, D. E. *Curr. Opin. Struct. Biol.* **2009**, *19*, 120−127.

(2) Shirts, M.; Pande, V. S. *Science* **2000**, *290*, 1903−1904.

(3) Abrams, C.; Bussi, G. *Entropy* **2013**, *16*, 163−199.

(4) Cino, E. A.; Choy, W.-Y.; Karttunen, M. *J. Chem. Theory Comput.* **2012**, *8*, 2725−2740.

(5) Vymětal, J.; Vondrášek, J. *J. Chem. Theory Comput.* **2012**, *9*, 441−451.

(6) Gerben, S. R.; Lemkul, J. A.; Brown, A. M.; Bevan, D. R. *J. Biomol. Struct. Dyn.* **2014**, *32*, 1817−1832 http://dx.doi.org/10.1080/07391102.2013.838518.

(7) Beauchamp, K. A.; Lin, Y.-S.; Das, R.; Pande, V. S. *J. Chem. Theory Comput.* **2012**, *8*, 1409−1414.

(8) Piana, S.; Klepeis, J. L.; Shaw, D. E. *Curr. Opin. Struct. Biol.* **2014**, *24*, 98−105.

(9) Lindorff-Larsen, K.; Maragakis, P.; Piana, S.; Eastwood, M. P.; Dror, R. O.; Shaw, D. E. *PLoS One* **2012**, *7*, e32131.

(10) Lange, O. F.; Van der Spoel, D.; De Groot, B. L. *Biophys. J.* **2010**, *99*, 647−655.

(11) Piana, S.; Lindorff-Larsen, K.; Shaw, D. E. *Biophys. J.* **2011**, *100*, L47−L49.

(12) Best, R. B.; Buchete, N.-V.; Hummer, G. *Biophys. J.* **2008**, *95*, L07−L09.

(13) Lindorff-Larsen, K.; Piana, S.; Palmo, K.; Maragakis, P.; Klepeis, J. L.; Dror, R. O.; Shaw, D. E. *Proteins: Struct., Funct., Bioinf.* **2010**, *78*, 1950−1958.

(14) Best, R. B.; Hummer, G. *J. Phys. Chem. B* **2009**, *113*, 9004−9015.

(15) Li, D.-W.; Brüschweiler, R. *Angew. Chem., Int. Ed.* **2010**, *122*, 6930−6932.

(16) Nerenberg, P. S.; Head-Gordon, T. *J. Chem. Theory Comput.* **2011**, *7*, 1220−1230.

(17) Kührová, P.; De Simone, A.; Otyepka, M.; Best, R. B. *Biophys. J.* **2012**, *102*, 1897−1906.

(18) Dyson, H. J.; Wright, P. E. *Nat. Rev. Mol. Cell. Biol.* **2005**, *6*, 197−208.

(19) Tompa, P. *Trends. Biochem. Sci.* **2012**, *37*, 509−516.

(20) Cui, Q.; Karplus, M. *Protein Sci.* **2008**, *17*, 1295−1307.

(21) Ma, B.; Tsai, C.-J.; Haliloglu, T.; Nussinov, R. *Structure* **2011**, *19*, 907−917.

(22) Palazzesi, F.; Barducci, A.; Tollinger, M.; Parrinello, M. *Proc. Natl. Acad. Sci. U. S. A.* **2013**, *110*, 14237−14242.

(23) De Simone, A.; Kitchen, C.; Kwan, A. H.; Sunde, M.; Dobson, C. M.; Frenkel, D. *Proc. Natl. Acad. Sci. U. S. A.* **2012**, *109*, 6951−6956.

(24) Barducci, A.; Bonomi, M.; Prakash, M. K.; Parrinello, M. *Proc. Natl. Acad. Sci. U. S. A.* **2013**, *110*, E4708−E4713.
(25) Krzeminski, M.; Marsh, J. A.; Neale, C.; Choy, W.-Y.; Forman-Kay, J. D. *Bioinformatics* **2013**, *29*, 398−399.
(26) Jensen, M. R.; Ruigrok, R. W.; Blackledge, M. *Curr. Opin. Struct. Biol.* **2013**, *23*, 426−435.
(27) Fisher, C. K.; Huang, A.; Stultz, C. M. *J. Am. Chem. Soc.* **2010**, *132*, 14919−14927.
(28) Camilloni, C.; Vendruscolo, M. *J. Am. Chem. Soc.* **2014**, *136*, 8982−8991.
(29) Dames, S. A.; Aregger, R.; Vajpai, N.; Bernado, P.; Blackledge, M.; Grzesiek, S. *J. Am. Chem. Soc.* **2006**, *128*, 13508−13514.
(30) Laio, A.; Parrinello, M. *Proc. Natl. Acad. Sci. U. S. A.* **2002**, *99*, 12562−12566.
(31) Barducci, A.; Bonomi, M.; Parrinello, M. *Wiley Interdiscip. Rev. Comput. Mol. Sci.* **2011**, *1*, 826−843.
(32) Best, R. B.; Mittal, J. *J. Phys. Chem. B* **2010**, *114*, 14916−14923.
(33) Jorgensen, W. L.; Chandrasekhar, J.; Madura, J. D.; Impey, R. W.; Klein, M. L. *J. Chem. Phys.* **1983**, *79*, 926.
(34) MacKerell, A. D.; et al. *J. Phys. Chem. B* **1998**, *102*, 3586−3616.
(35) Abascal, J. L.; Vega, C. *J. Chem. Phys.* **2005**, *123*, 234505.
(36) Hornak, V.; Abel, R.; Okur, A.; Strockbine, B.; Roitberg, A.; Simmerling, C. *Proteins: Struct., Funct., Bioinf.* **2006**, *65*, 712−725.
(37) Earl, D. J.; Deem, M. W. *Phys. Chem. Chem. Phys.* **2005**, *7*, 3910−3916.
(38) Bonomi, M.; Parrinello, M. *Phys. Rev. Lett.* **2010**, *104*, 190601.
(39) Barducci, A.; Bussi, G.; Parrinello, M. *Phys. Rev. Lett.* **2008**, *100*, 020603.
(40) Camilloni, C.; Cavalli, A.; Vendruscolo, M. *J. Chem. Theory Comput.* **2013**, *9*, 5610−5617.
(41) Burney, P. R.; White, N.; Pfaendtner, J. *PLoS One* **2014**, *9*, e86981.
(42) Frishman, D.; Argos, P. *Proteins: Struct., Funct., Bioinf.* **1995**, *23*, 566−579.
(43) Karplus, M. *J. Am. Chem. Soc.* **1963**, *85*, 2870−2871.
(44) Wang, A. C.; Bax, A. *J. Am. Chem. Soc.* **1996**, *118*, 2483−2494.
(45) Hu, J.-S.; Bax, A. *J. Am. Chem. Soc.* **1997**, *119*, 6360−6368.
(46) Barducci, A.; Bonomi, M.; Parrinello, M. *Biophys. J.* **2010**, *98*, L44−L46.
(47) Han, B.; Liu, Y.; Ginzinger, S. W.; Wishart, D. S. *J. Biomol. NMR* **2011**, *50*, 43−57.
(48) Robustelli, P.; Stafford, K. A.; Palmer, A. G., III *J. Am. Chem. Soc.* **2012**, *134*, 6365−6374.
(49) Wishart, D. S.; Case, D. A. *Methods Enzymol.* **2000**, *338*, 3−34.
(50) Jensen, M. R.; Markwick, P. R.; Meier, S.; Griesinger, C.; Zweckstetter, M.; Grzesiek, S.; Bernado, P.; Blackledge, M. *Structure* **2009**, *17*, 1169−1185.
(51) Zweckstetter, M.; Bax, A. *J. Am. Chem. Soc.* **2000**, *122*, 3791−3792.
(52) Sgourakis, N. G.; Merced-Serrano, M.; Boutsidis, C.; Drineas, P.; Du, Z.; Wang, C.; Garcia, A. E. *J. Mol. Biol.* **2011**, *405*, 570−583.
(53) Ohnishi, S.; Lee, A. L.; Edgell, M. H.; Shortle, D. *Biochemistry* **2004**, *43*, 4064−4070.
(54) Hess, B.; Kutzner, C.; van der Spoel, D.; Lindahl, E. *J. Chem. Theory Comput.* **2008**, *4*, 435−447.
(55) Bonomi, M.; Branduardi, D.; Bussi, G.; Camilloni, C.; Provasi, D.; Raiteri, P.; Donadio, D.; Marinelli, F.; Pietrucci, F.; Broglia, R. A.; Parrinello, M. *Comput. Phys. Commun.* **2009**, *180*, 1961−1972.
(56) Prakash, M. K.; Barducci, A.; Parrinello, M. *J. Chem. Theory Comput.* **2011**, *7*, 2025−2027.
(57) Bonomi, M.; Barducci, A.; Parrinello, M. *J. Comput. Chem.* **2009**, *30*, 1615−1621.
(58) Deighan, M.; Bonomi, M.; Pfaendtner, J. *J. Chem. Theory Comput.* **2012**, *8*, 2189−2192.
(59) Brüschweiler, R.; Case, D. *J. Am. Chem. Soc.* **1994**, *116*, 11199−11200.
(60) Case, D. A.; Scheurer, C.; Brüschweiler, R. *J. Am. Chem. Soc.* **2000**, *122*, 10390−10397.
(61) Markwick, P. R.; Showalter, S. A.; Bouvignies, G.; Brüschweiler, R.; Blackledge, M. *J. Biomol. NMR* **2009**, *45*, 17−21.
(62) Grossfield, A.; Zuckerman, D. M. *Annu. Rep. Comput. Chem.* **2009**, *5*, 23−48.